Biochimica et Biophysica Acta 1837 (2014) 1196–1207

Contents lists available at ScienceDirect

Biochimica et Biophysica Acta

journal homepage: www.elsevier.com/locate/bbabio

Review

The role of protein dynamics and thermal fluctuations in regulating cytochrome *c*/cytochrome *c* oxidase electron transfer☆

Damian Alvarez-Paggi, Ulises Zitare, Daniel H. Murgida *

INQUIMAE-CONICET, Departamento de Química Inorgánica, Analítica y Química Física, Facultad de Ciencias Exactas y Naturales, Universidad de Buenos Aires, Ciudad Universitaria, pab. 2, piso 3, C1428EHA Buenos Aires, Argentina

ARTICLE INFO

Article history:
Received 22 November 2013
Received in revised form 22 January 2014
Accepted 28 January 2014
Available online 3 February 2014

Keywords:
Cytochrome c
CuA
Bioelectrochemistry
Raman spectroelectrochemistry
Electron transfer

ABSTRACT

In this overview we present recent combined electrochemical, spectroelectrochemical, spectroscopic and computational studies from our group on the electron transfer reactions of cytochrome *c* and of the primary electron acceptor of cytochrome *c* oxidase, the Cu_A site, in biomimetic complexes. Based on these results, we discuss how protein dynamics and thermal fluctuations may impact on protein ET reactions, comment on the possible physiological relevance of these results, and finally propose a regulatory mechanism that may operate in the Cyt/CcO electron transfer reaction *in vivo*. This article is part of a Special Issue entitled: 18th European Bioenergetic Conference.

1. Introduction

Proteins are highly dynamic entities that at physiological temperatures explore hyperdimensional free energy surfaces (FES), thereby sampling a rich conformational space [1,2]. These FES present a hierarchy of energy wells and barriers that determine a wide range of fluctuations, from atomic vibrations to collective distortions of secondary and tertiary structures, with associated timescales from picoseconds to milliseconds [3]. Post-translational modifications, local electric fields, protonation of titrable residues, ligand binding and protein–protein interactions, among other perturbations, can dynamically reshape the FES, thus allowing proteins to sample conformations that enable functions that can only be performed while oscillating around specific FES minima. This structure–dynamics–function paradigm is also suitable for the rationalization of protein electron transfer (ET) reactions. Indeed, control of electron transfer kinetics by fast and slow protein dynamics has been reported and theoretically modeled for a variety of systems [4–16].

In this article we focus on recent experimental and computational studies from our lab aiming to understand the role of slow protein dynamics and electrostatic interactions in regulating the ET reactions of cytochrome *c* (Cyt) and of the primary electron acceptor of cytochrome *c* oxidase (CcO), the Cu_A center (Fig. 1).

Long range (non-adiabatic) biological ET reactions are usually interpreted in terms of Marcus' theory [19,20] and subsequent extensions by Hush, Jortner, Dogonadze, Kuznetsov and others [21–26]. Within this theoretical framework, nuclear coordinates of donor (*D*) and acceptor (*A*) are considered to fluctuate along the reaction coordinate until *D*/*A* electronic energies match each other, thereby making electron tunneling a quantum mechanically allowed process.

The relevant parameters that determine the ET rate constant, k_{ET}, are the free energy of the reaction, ΔG, the free energy of activation, $\Delta G^{\ddagger}$, the closely related reorganization energy, λ, the D/A electronic coupling H_{DA} and the temperature, *T*:

$$k_{ET} = \frac{2\pi}{\hbar}|H_{DA}|^2 \frac{1}{\sqrt{4\pi\lambda k_B T}} \exp\left(-\frac{(\Delta G+\lambda)^2}{4\lambda k_B T}\right). \quad (1)$$

Here the driving force of the reaction, ΔG, is determined by the *D*/*A* redox potentials E^0, $|H_{DA}|^2$ represents the probability of electron tunneling between the degenerate states and λ is the (hypothetical) change of free energy if the reactants state were to distort to the equilibrium nuclear configuration of the products state without actual transfer of the electron. In classical Marcus theory $\Delta G^{\ddagger} = (\Delta G + \lambda)^2/4\lambda$). It is important to stress that most structure-based ET coupling theories include parameters describing details of the *D*/*A* state electronic structure [27,28]. However, information needed to assess these parameters is unknown in most cases, and treatments often assume only one donor (and acceptor) electronic wave function involved, *i.e.*, the so called redox-active molecular orbital (RAMO), thereby emphasizing the role of the bridge. It has been shown that structural fluctuations of the bridge between *D* and *A* modulate H_{DA}, leading to different regimes depending on the time

☆ This article is part of a Special Issue entitled: 18th European Bioenergetic Conference.
* Corresponding author.
E-mail address: dhmurgida@qi.fcen.uba.ar (D.H. Murgida).

http://dx.doi.org/10.1016/j.bbabio.2014.01.019
0005-2728/

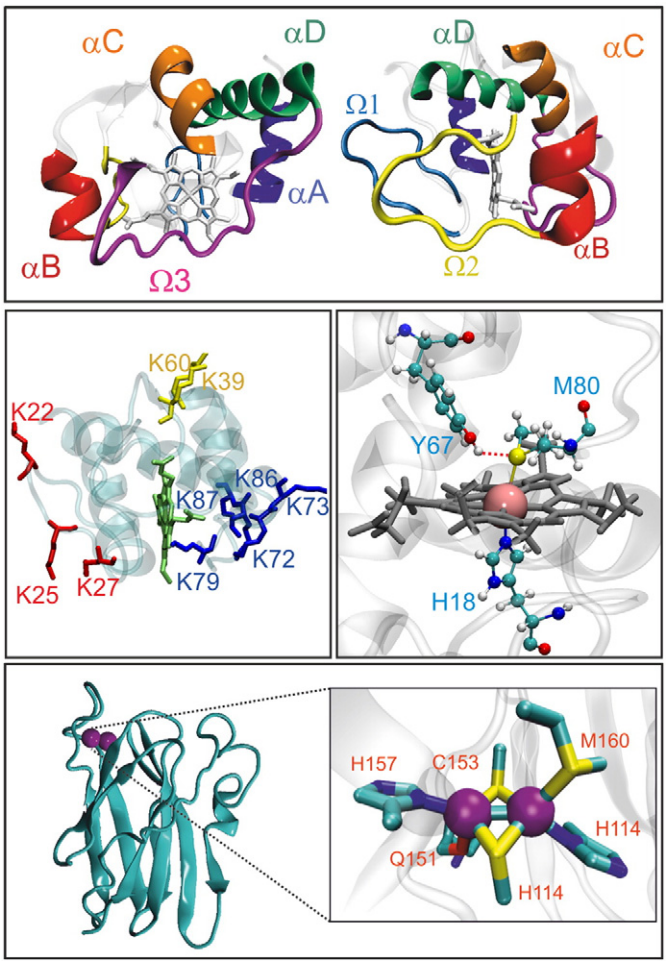

Fig. 1. Top: Structure of horse heart cytochrome *c* highlighting the secondary structure motifs consisting of 4 alpha helixes and 3 Ω loops. Middle: Cytochrome *c* residues relevant to the present discussion. Bottom: Structure of the soluble fragment from subunit II of the cytochrome ba_3 oxidase from *T. thermophilus* (left) and detailed view of the Cu_A center (right). The structures have been adapted from PDB files 1HRC [17] and 2CUA [18], respectively.

scale of the fluctuations with respect to the lifetime of the resonant *D/A* state [9,29]. The structural features of the protein (and water) bridging *D* and *A* define the tunneling rates, even for large coupling fluctuations [30,31].

Redox centers in metalloproteins are embedded in fluctuating amino acidic matrixes that dynamically modulate the electronic properties of the site through first, second and higher order metal coordination and through the local electrostatic potential. Moreover, interactions between redox partners in reactive complexes may result in further perturbations of the protein scaffold that may impact on the redox centers and, at the same time, impose geometric constrains on protein dynamics. While all of these variables and processes may potentially modulate the ET reactions trough thermodynamic and kinetic parameters such as E^0, λ and H_{DA}, detailed studies under reactive conditions and atomistic resolution of these complex systems are far from trivial, thus making progress in this area relatively slow.

In this respect, redox proteins adsorbed on electrodes coated with biomimetic films represent simplified model systems that offer a unique opportunity for performing detailed and well controlled physicochemical studies under reactive conditions. Using this strategy we have investigated the heterogeneous ET dynamics of Cyt and Cu_A employing protein film voltammetry and time-resolved surface-enhanced resonance Raman techniques as the main experimental tools, in combination with molecular dynamics (MD) simulations and quantum mechanical (QM) calculations. Our aim is to elucidate the effect of slow protein dynamics and electrostatic interactions on different kinetic, structural and electronic parameters that determine the efficiency and directionality of the ET reactions of Cyt and Cu_A.

The next three sections summarize the main results obtained about modulation of the ET pathways, reorganization energies and redox active molecular orbitals. Finally, based on these results, we postulate a novel regulatory mechanism that may operate in the Cyt/CcO ET reaction *in vivo* and that might be relevant for the regulation of electron–proton energy transduction in general.

2. Modulation of the electronic coupling of Cyt by protein dynamics

Protein dynamics has been early recognized as a key factor in controlling inter-protein ET rates. For example, multiphasic kinetics of the reaction between photosystem I and plastocyanin as well as bell-shaped ionic strength dependencies of the reaction kinetics between Cyt and CcO were interpreted in terms of reorientation of the protein/protein complexes as a prerequisite for efficient electron tunneling [32,33]. These pioneering studies, however, did not provide direct evidence of the reorientation step. Latter NMR experiments provided deeper insight into the dynamics of inter-protein complexes, albeit under non-reactive conditions [34–37].

A seemingly unrelated experimental phenomenon provided a unique opportunity to directly investigate and disentangle electron tunneling and protein reorientation under reactive conditions. Electrochemists have, for over 20 years now, studied redox proteins adsorbed on metal electrodes coated with self-assembled monolayers (SAMs) of ω-functionalized alkanethiols [38–40]. These biomimetic or biocompatible films are exceptionally versatile, as they allow for controlling the type of interactions established with the protein and the electron tunneling distances through selection of the tail groups and chain lengths of the constituent alkanethiols, respectively. For such systems Eq. (1) has to be integrated to account for the density of states of the metal according to [41]:

$$k_{ET}(\eta) = \frac{2\pi}{\hbar}|H_{DA}|^2 \int_{-\infty}^{\infty} \frac{1}{1+\exp\left(\frac{\epsilon-\epsilon_f}{k_BT}\right)} \rho(\epsilon) \frac{1}{\sqrt{4\pi\lambda k_BT}} \exp\left[-\frac{(\lambda - e\eta + \epsilon)^2}{4\lambda k_BT}\right] d\epsilon \quad (2)$$

where η is the electrode overpotential relative to the protein redox potential, $\rho(\epsilon)$ is the density of electronic states in the metal electrode and ϵ_f is the energy of the Fermi level. The electronic coupling between the protein redox center at a particular fixed orientation and the metal, $|H_{DA}|$, is expected to decay exponentially with the number of $-CH_2-$ groups (n) of the SAMs with a characteristic coupling decay parameter β [42,43]:

$$|H_{DA}| = \left|H_{DA}^0\right| exp(-\beta n). \quad (3)$$

This behavior has been verified for a number of small redox active molecules. For proteins, in contrast, the prediction is usually confirmed for relatively thick SAMs (typically $n > 10$) but fails at thinner films, where k_{ET} appears to be insensitive to the tunneling distance. This "unusual" response was observed for a wide variety of redox centers including Cyt, *iso*-Cyt, Cyt-c_6, Cyt-b_{562}, azurin, plastocyanin and Cu_A centers on different SAMs and metals (Fig. 2) [44–57]. Different hypotheses have been proposed to rationalize this rather ubiquitous behavior depending on the specific case. Here we will focus only in the case of Cyt electrostatically adsorbed on negatively charged SAMs. For this case Avila and coworkers were the first to suggest a gating step based on the transition from a redox inactive to a redox active protein orientation [44]. This two-state minimal model, however, is based on indirect evidence and does not account for the nature of the active and inactive species and the role of the applied potential.

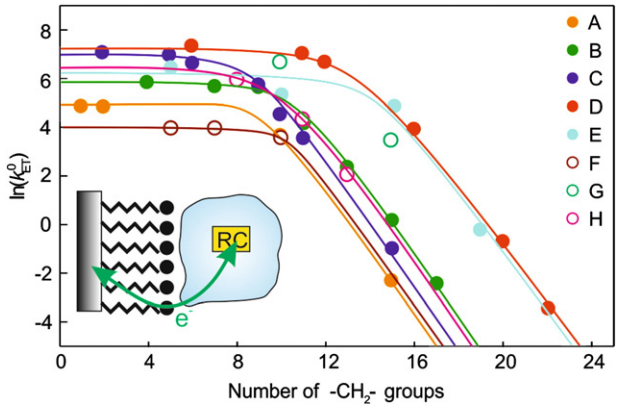

Fig. 2. Distance-dependencies of the apparent ET rate constants for different proteins immobilized of SAM-coated metal electrodes. A: Cyt on CO_2^--terminated SAM coated Ag electrodes.[48,51,52] B: Cyt on CO_2^--terminated SAM coated Au electrodes.[44,46,47,54] C: Azurin on CH_3-terminated SAM coated Au electrodes.[45] D: Cyt on pyridine-terminated SAM coated Au electrodes.[53,55] E: Cyt domain from the cytochrome caa_3 oxidase from *Rhodotermus marinus* on mixed CH_3/OH terminated SAM coated Ag electrodes.[50] F: Cyt-b_{562} on NH_3^+-terminated SAM coated Ag electrodes.[56] G: Cyt-c_6 on mixed CH_3/OH terminated SAM coated Ag electrodes.[49] H: Soluble fragment from the subunit II of the cytochrome ba_3 oxidase from *Thermus thermophilus* on mixed CH_3/OH terminated SAM coated Ag electrodes.[57].

The first direct evidence of protein reorientation as the gating step was recently obtained from time-resolved surfaced-enhanced resonance Raman (TR-SERR) spectroelectrochemical experiments [16]. Resonance Raman spectra (RR) of heme proteins are very sensitive to the redox state, spin and axial coordination of the heme iron, as well as to protein–cofactor interactions [58–60]. When the protein is adsorbed on SAM-coated nanostructured Ag electrodes the RR signal is greatly intensified due to electromagnetic surface enhancement of the incoming and scattered photons. In addition to a drastic gain of sensitivity, the surface enhancement effect presents the advantage of providing orientational information. This is so because the individual components of the Raman scattering tensor are affected to different extents depending on the direction of the electric-field vector relative to the heme plane, such that vibrational modes of different symmetry will undergo differential intensifications for each protein orientation [61]. For example, A_{1g} modes will experience preferential enhancement when the heme plane is parallel to the plasmonic surface, while for perpendicular orientations A_{1g} and B_{1g} modes will both be enhanced (Fig. 3).

Therefore, changes of A_{1g}/B_{1g} relative intensities constitute a direct measurement of protein re-orientation in the biomimetic complexes. In TR-SERR spectroelectrochemical experiments the adsorbed protein is first equilibrated at a given initial potential and, afterwards, it is suddenly perturbed by a potential step of variable amplitude and duration [62]. SERR spectral changes recorded at different delay times with respect to the potential step provide simultaneous information on the

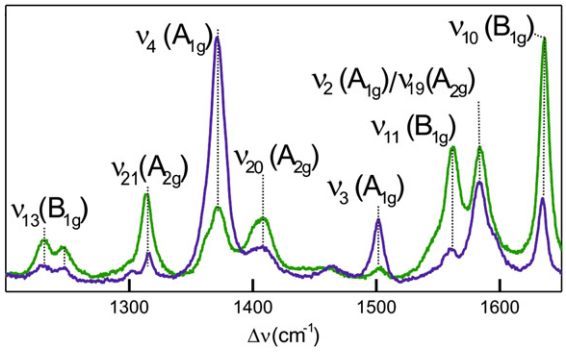

Fig. 3. SERR spectra of ferric Cyt recorded under Soret (violet) and Q-band (green) excitation.

progress of the ET reaction and of possible redox-linked structural changes at the level of the heme pocket, while directly monitoring protein reorientation in the assemblies over a broad time window, from microseconds to minutes. While TR-SERR spectra recorded under Soret-band excitation provide the highest sensitivity and are preferred for monitoring ET and structural dynamics, Q-band excitation allows for more reliable determinations of orientational dynamics [16,60].

Application of this experimental strategy to Cyt adsorbed on nanostructured Ag electrodes coated with SAMs of ω-carboxyl alkanethiols of variable length was quite revealing. We observed that at thick SAMs, for which the expected exponential distance-dependence of k_{ET} is verified, potential-induced protein reorientation in the assemblies is several orders of magnitude faster than electron tunneling. At shorter tunneling distances ($n < 10$), instead, we found two remarkable features: (i) ET and protein reorientation rate constants (k_{ET} and k_r, respectively) are almost identical and (ii) protein reorientation is orders of magnitude slower than at thicker SAMs (Fig. 4) [16].

While these results constitute compelling direct evidence of protein reorientation as the rate determining gating step at short tunneling distances, they poise additional questions, such as why Cyt needs to reorient in order to efficiently transfer electrons and why the reorientation dynamics is itself distance-dependent. A combination of theoretical and experimental results shed light on these matters [63–65].

At physiological pH Cyt has net positive charge determined by a ring of protonated lysine residues surrounding the partially exposed heme edge [17]. This positive patch establishes electrostatic contacts with negative counterparts in biomimetic and natural complexes, thus determining the coarse protein orientation. In addition, Cyt presents a dipole moment of *ca* 340 debye that, in the presence of electric fields, influences the orientation and rotational dynamics of the protein [63,66].

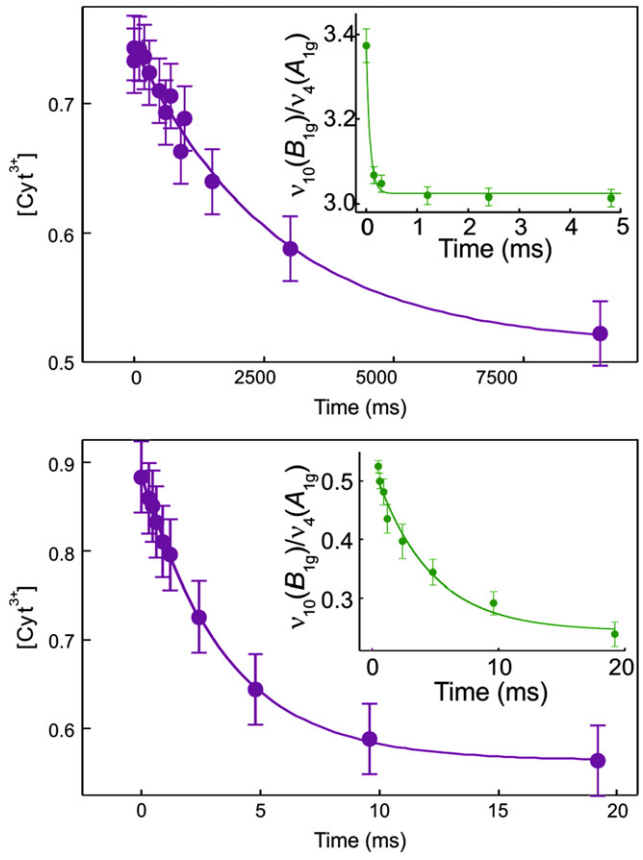

Fig. 4. Electron transfer (violet) and reorientation (green) dynamics of Cyt adsorbed on SAMs of ω-carboxyl alkanethiols with 15 (top) and 5 (bottom) $-CH_2-$ groups, monitored by TR-SERR spectroelectrochemistry under Soret (violet) and Q-band (green) excitation, adapted from Kranich et al.[16].

In this respect, the artificial metal electrode/SAM/solution interfaces reproduce some essential characteristics of the biological solution/lipid bilayer/solution interfaces, specifically the existence of strong local electric fields. While at biological membranes they arise from contributions of dipole, surface and Donnan potentials, [67] in the metal electrode they originate in the potential drop across the SAM, and its magnitude is determined by the potential of zero charge of the metal, the applied potential, the tail groups and chain length of the SAMs and the electrolyte composition. For SAMs of ω-carboxyl alkanethiols on Ag electrodes at neutral pH and electrode potentials close to the E^0 value of Cyt the interfacial electric field can be modulated between 0.01 and 0.1 V $Å^{-1}$, [58,59,68] *i.e.* very close to the upper values predicted for lipid bilayers [67]. Moreover, the field intensity can be easily varied trough the chain length of the alkanethiol without altering any other parameter; thinner SAMs correspond to stronger local fields and *vice versa*. These considerations allow rationalizing the experimental observation of slower rotational dynamics of Cyt at thinner SAMs. Further support to this interpretation comes from the fact that k_r increases with decreasing pH within a range (7.8 to 6) that affects protonation of the SAM more dramatically than that of the protein and, therefore, the acceleration is consistent with weaker interfacial electric fields. It is important to point out that k_{ET} and k_r remain identical at all pH values when Cyt is adsorbed on thin SAMs. Consistently, a 20% increase of the solution viscosity under these conditions reduces both rate constants by a factor of 2, confirming that rotational dynamics is the rate limiting event of the overall redox reaction [16].

To gain deeper insight into the atomistic details of the process we investigated the Cyt/SAM/electrode complex by means of molecular dynamics (MD) simulations [63,65]. At first place we computed the adsorption of Cyt to the SAMs starting from 20 different possible orientations. All the stable electrostatic complexes found were further subjected to 20 ns simulations in explicit solvent, thus allowing the systems to sample a large number of conformations, comprising not only coarse protein orientation but also more subtle differences, such as the conformation of amino acidic side chains, the structure and arrangement of the interfacial water molecules and subtle deformations of the heme cofactor. The energetics of all the thermally accessible protein-SAM conformations was assessed by using the MM/PBSA approximation. The results show that the protein is able to explore a relatively broad range of orientations as determined by two characteristic angles, α and φ. These angles represent the tilt of the heme plane with respect to electrode surface and the rotation of the asymmetric porphyrin ring around the imaginary perpendicular axis that contain the Fe atom, respectively. As shown in Fig. 5, the protein explores a range of approximately 70° both in α and φ. Other orientations are possible, but their binding energies are too small to achieve significant populations at room temperature.

Careful inspection of the simulated complexes reveals that Cyt/SAM contacts involve the same lysine residues implicated in complexes with natural redox partners such as CcO, cytochrome *c* peroxidase and bc_1 complex, [63,69–71] thus validating the biomimetic characteristics of the model system employed.

Computation of the electronic coupling decays (D^H) along the dynamics by means of the *pathways* algorithm [72,73] yields quite reveling results: those orientations that are energetically more favorable present very low electronic couplings, thereby implying that Cyt reorientation is required to attain efficient electron pathways (Fig. 5). Besides coarse protein orientation, subtle fluctuations such as the movement of interfacial water molecules and side-chain rearrangements may also impact deeply in the coupling. For instance, Fig. 6 shows that H_{DA} may increase by nearly one order of magnitude without significant protein reorientation due to pathway short-circuiting by a water molecule.

This theoretical prediction was experimentally verified when studying the ET dynamics of Cyt covalently attached to carboxyl-terminated SAMs [64]. Although in this case coarse protein reorientation was hindered, the anomalous distance dependence was still verified, albeit

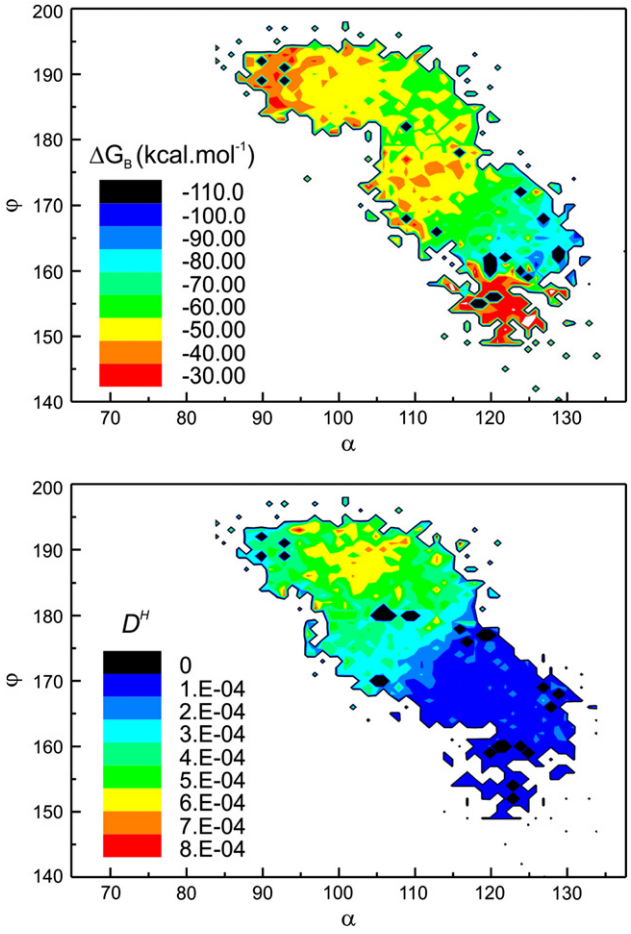

Fig. 5. Top: Binding free energy (ΔG_B) of Cyt adsorbed on a SAM of ω-carboxyl alkanethiol as a function of protein orientation. Bottom: Electronic coupling decay (D^H) calculated at the explored orientations of Cyt. Adapted from Alvarez-Paggi et al. [63].

with lower k_{ET} limiting values. Thus, the theoretical and experimental results suggest that both coarse and fine dynamics are strongly affected by interfacial electric fields of biologically relevant magnitude. To further test this hypothesis we constructed the K87C mutant that, according to the calculations, should abolish contacts that stabilize low electronic coupling orientations [74]. In excellent agreement with the theoretical predictions, TR-SERR and CV experiments show that the effect of such mutation is eliminating the rate limiting character of protein dynamics as evidenced by the recovery of an exponential distance dependence of k_{ET} for all chain lengths (Fig. 7), *i.e.* consistent with a non-gated diabatic (long range) ET reaction.

In summary, the obtained experimental and computational results demonstrate that the electronic coupling of Cyt is strongly modulated by large and small amplitude dynamics of the protein and interfacial water molecules in the electrostatic complexes. Both types of fluctuations are influenced by local electrostatic fields of biologically relevant magnitude that constitute the basis of the gating step in long range ET reactions.

2.1. Modulation of the reorganization energy of Cyt by electrostatic interactions

The structural details and fluctuations of the protein bridging two redox centers are crucial in mediating H_{DA}, as extensively and controversially discussed in the literature. Another rate-accelerating mechanism evolved by nature is the ability of the protein and redox site structure to minimize the activation barrier ($\Delta G^{\ddagger}$) for achieving degeneracy of the electronic initial and final states of the reaction.

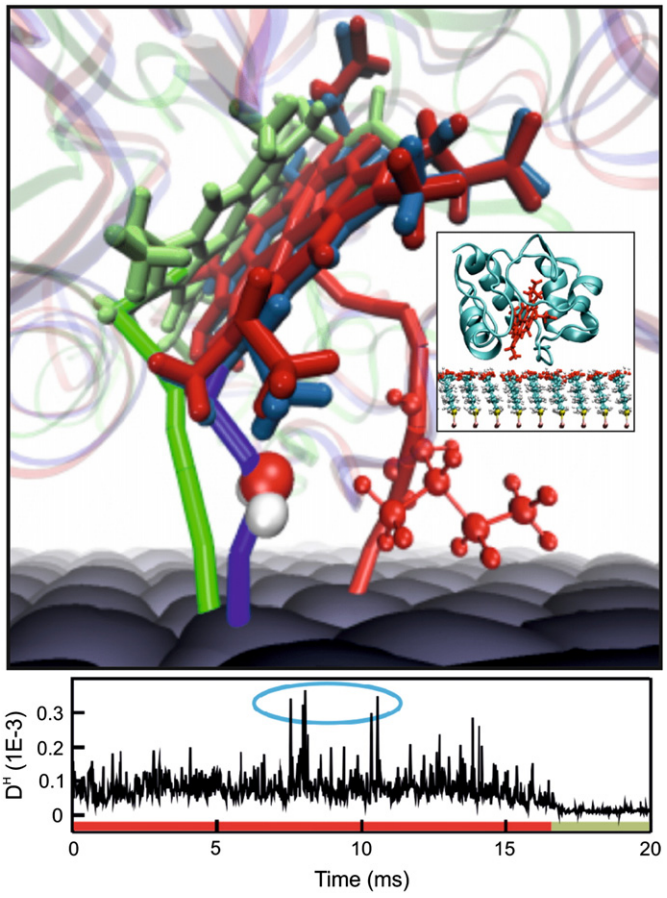

Fig. 6. Water-mediated increase of the electronic coupling observed during a 20 ns MD of Cyt adsorbed on SAM coated electrodes. Preferred electronic pathways for Cyt in two slightly different orientations are shown in red and green. Transient positioning of water molecules establish high coupling pathways, as indicated in blue. Adapted from Alvarez-Paggi et al. [63].

A completely equivalent way to analyze this aspect in terms of Marcus theory is through the reorganization free energy λ [75]. This parameter can be divided into inner and outer sphere contributions: λ_{in} and λ_{out}, respectively. For metalloproteins λ_{in} is mainly determined by redox-linked structural changes within the first coordination sphere, and thus it is minimized by metal sites that exhibit very small structural differences between the reduced and oxidized forms, and that are enclosed in a hydrophobic protein environment [76–81]. Rearrangements of the remainder of the protein and the environment are comprised in λ_{out} [82]. Thus, it can be anticipated that λ_{out} is minimized by a rigid protein

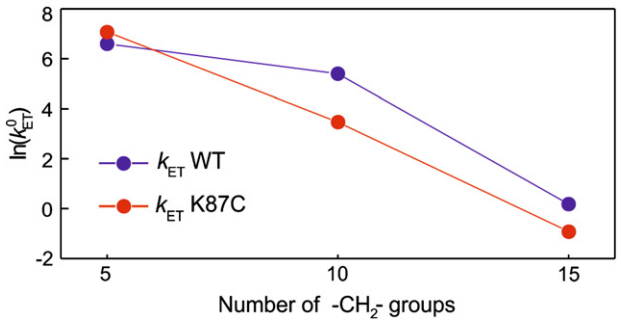

Fig. 7. Distance dependence of k_{ET} for Cyt WT and the K87C mutant adsorbed on SAM coated electrodes. For the K87C mutant, the dependence is exponential, in contrast to the onset of the *plateau* region for Cyt WT at short SAMs. Adapted from Alvarez-Paggi et al.[74].

matrix and by a hydrophobic protein interior that effectively shields the redox site from solvent water molecules and minimizes the dielectric response to changes of the metal charge [81]. Indeed, it has been shown that reducing solvent accessibility to the redox site and to the protein surface lowers the value of λ_{out} [64,83]. Establishing the relative magnitudes and cut off between the λ_{in} and λ_{out} terms, however, is far from trivial. Even less established is the possible modulation of λ through mechanisms such as protein–protein interactions or membrane potentials [59,81,84]. These issues are of utmost importance, for instance, for understanding the origin of fast ET reactions involved in biological electron–proton energy transduction [85,86].

Neglecting the dynamical nature of the protein structure renders interpretation of experimental data and theoretical calculations quite unsuccessful. Many hypotheses were proposed regarding the factors that determine the reorganization energy of Cyt. However none of them were capable of rationalizing the whole span of values presented in the literature ranging from 0.22 to 1.1 eV, [87–94] and even more extreme values [95]. Such dispersion could be caused, to some degree, by the experimental difficulties associated with λ determinations, but they could also hint at a complicated regulatory scheme that may be at play and unknowingly perturbed by the different experimental techniques. The role of the protein matrix in minimizing λ of Cyt compared to the free porphyrin was early recognized [96]. Later studies focused on the effect of disrupting the protein matrix either by addition of denaturing agents or by point mutations [92]. It was found, for instance, that the value of λ rises in a sigmoidal fashion with increasing concentrations of urea due to augmented solvent exposure of the metal site in the partially unfolded protein. This effect is observed in the range of 5–8 M urea that onsets a small structural transition that precedes a larger one taking place at urea concentrations of ca. 9 M, the latter involving major structural rearrangements such as exchange of the iron axial ligand M160 for a His residue. The increased solvent accessibility and the subsequent alteration of the coordination pattern impact on λ_{out} and λ_{in}, respectively [92]. Along the same lines, Bortolotti and coworkers studied various single, double and triple Cyt mutants and found that experimental and theoretically calculated values of λ exhibit a linear correlation with the computationally calculated solvent accessible surface area of the heme for λ values from *ca* 0.39 to 0.48 eV [83].

While these results represent a key contribution for understanding how the reorganization energy of Cyt is kept low, they do not explain the wide dispersion of experimental values reported in the literature. Usually, when considering λ, much emphasis is put on the protein matrix in terms of solvent accessibility, while little attention is paid to the structure of the heme-iron moiety as long as the first coordination sphere is preserved. In-between, the fine nexus that couples outer and inner sphere elements is often neglected. We paid specific attention to such matters, focusing on the interaction between the first and second sphere iron ligands M80 and Y67 because Y67 has been proposed to be crucial in controlling Cyt structure and function through an extended H-bonding network [97]. However, H-bonding between Y67 and M80 has been a controversial issue and is often inferred based solely on visual inspection of crystal structures or from extrapolation of indirect evidences obtained for Cyt variants from different organisms [98–102]. Recent MD simulations on human Cyt refuted this interaction, [103] but the search algorithms employed in these simulations were not optimized for H-bonds in which the acceptor is an S atom. In a recent study of over 500 proteins, Zhou et al. demonstrated that the characteristic angles and distances (Fig. 8) for these cases differ widely from those corresponding to canonical H-bonding interactions [104].

Therefore, we analyzed the Y67–M80 interaction using MD simulations and a home-made search algorithm that implements Zhou's parameters [105]. The results showed that, although a relatively weak and fluctuating interaction, Y67 and M80 can be regarded as H-bonded (Fig. 8). Moreover, this interaction might couple structural rearrangements of the protein matrix and the heme group, thus blurring the line of what is considered inner and outer sphere. This

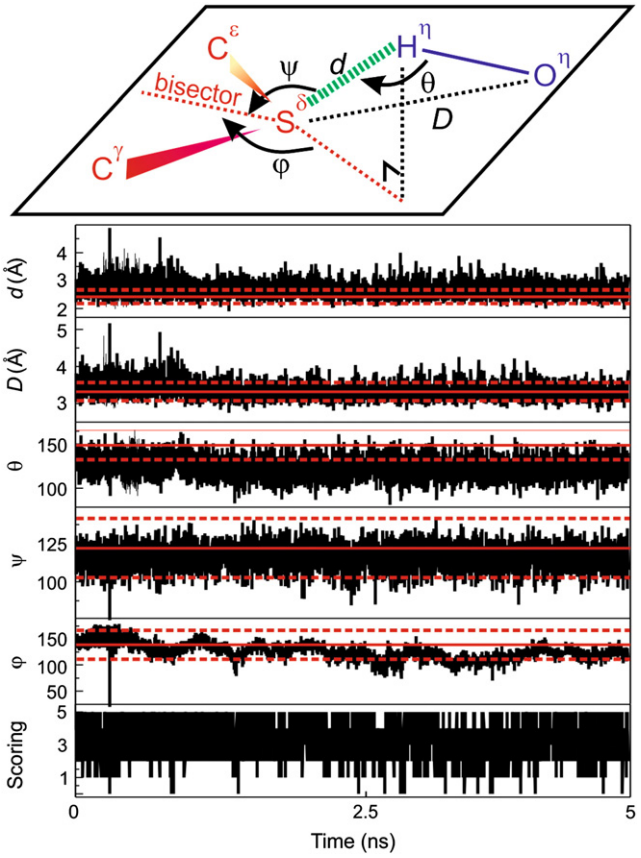

Fig. 8. Top: Geometric parameters for defining an H bond interaction with an S atom from a methionine as the acceptor, adapted from Zhou et al. [104]. Bottom: Evaluation of each of the geometric parameters and scoring factor for the Y67-M80 H bond interaction from a 5 ns MD simulation, showing the establishment of said interaction. The red lines indicate the average (full) and standard deviation (dotted) values for this type of H bond interaction. The scoring factor, ranging from 0 to 5, represents the number of structural parameters that lie within the corresponding confidence interval. Adapted from Alvarez-Paggi et al. [105].

finding prompted us to perform comparative experimental studies of WT Cyt and the Y67F mutant, which preserves the overall folding, structure and function of the WT variant but lacks the H-bond to M80. Specifically we determined k_{ET} for both protein variants adsorbed on electrodes coated with SAMs containing variable proportions of carboxyl ω-substitutes, *i.e.* variable charge density. Electrochemical (CV) and spectroelectrochemical (TR-SERR) determinations were performed (i) as a function of temperature and (ii) at fixed temperature and variable overpotential, to extract reliable λ values in two independent ways (Eq. (2)). For the WT protein we obtained λ = 0.4 eV for SAMs with high charge density and λ = 0.5 eV for low charge density. In contrast, the Y67F mutant is insensitive to the charge density of the SAM yielding λ = 0.4 eV in all cases, thus suggesting that the Y67-M80 H-bond renders the kinetic ET parameters of WT Cyt sensitive to electrostatic interactions.

Complementary MD simulations show that for Cyt adsorbed to weakly charged SAMs the secondary structure elements and RMSD values are nearly identical to the protein in solution, although the H-bond weakens (Fig. 9). As the charge density of the SAM increases, the secondary structure elements remain mostly unaltered, but the RMSD increases in segments corresponding to two well-defined Ω loops (residues 20–30 and 70–85; Fig. 1). These results are in remarkably good agreement with those obtained for the iso-1-Cyt/cytochrome bc_1 complex, [106] where it was found that the Ω loop containing residues 20–30 is the most susceptible to structural variations. Moreover, we found that the aforementioned changes further weaken the M80-Y67 H-bond. Weakening of the H-bond appears to be

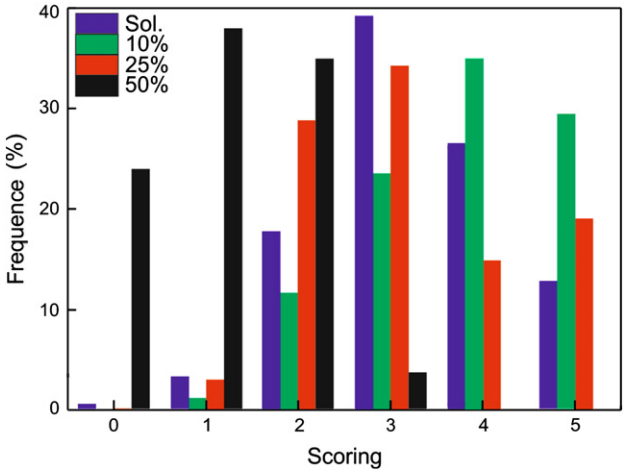

Fig. 9. Histogram of the scoring function of the Y67-M80 interaction for 5 ns MD simulations of Cyt in solution and adsorbed on carboxyl-terminated SAMs of increasing degree of deprotonation (10%, 25% and 50%). As the charge density increases, the frequency of the lower scoring values increases, indicative of the disruption of the Y67-M80 bond. Adapted from Alvarez-Paggi et al. [105].

independent of the redox state of Cyt, thus suggesting a predominant role of small collective structural perturbations of the protein matrix.

The Ω loops that undergo deformations contain the majority of the lysine residues involved in establishing electrostatic contacts with the SAMs and with the natural redox partners of Cyt, such as mitochondrial complexes III and IV and cytochrome *c* peroxidase (Fig. 1) [69–71]. Remarkably, per residue RMSDs of Cyt adsorbed on SAMs are similar to those of Y67F in solution, thus suggesting that this mutation and electrostatic interactions trigger similar conformational transitions of Cyt. These results indicate that the Y67/M80 H-bond is a key element of the conformational switch between high and low λ forms of native Cyt. We propose that this transition arises from the collective perturbation of the dynamics and average position of the amino acidic residues and nearby water structural molecules, and that this dynamical change is achievable through the disruption of the Y67-M80 bond [105].

The fact that the interruption of the Y67-M80 H-bond achieved either by Y67F mutation or by electrostatic interactions of WT Cyt do actually minimize λ to similar extents, underlies the involvement of this relatively weak interaction between first- and second-sphere ligands in stabilizing the high λ form. The conformational change between the high and low λ forms of Cyt is activated by deformations of the flexible Ω loops that contain most of the lysine residues which constitute the protein binding site. We propose that a similar mechanism could be triggered upon interactions of Cyt with the natural redox partners, CcO and Cyt-bc1, thus minimizing the reorganization energy for inter-protein ET. Indeed, the interactions between Cyt and natural partner proteins involve the same lysine residues implicated in the model electrostatic complexes [63,69–71].

Last but not least, these findings allow rationalizing the dispersion of λ values previously reported for Cyt as the average value of λ obtained for protein samples in solution (analogous to a low interfacial charge density) is ca. 0.6 eV, [89,90,92,94] but it reduces to ca. 0.3 eV in electrostatic complexes [91,93]. In addition, our results consistently explain the experimental values reported for cytochromes from different organisms depending on the presence or absence of the Y67-M80 H bond interaction and on the experimental conditions employed [94,107].

3. Alternative redox active ground states of Cu_A

The geometric and electronic properties of the Cu_A site were matter of controversy for over 30 years mainly due to inherent experimental complications [108]; the main one being that cytochrome *c* oxidases

(and N_2O reductases) are multimeric proteins that contain several spectroscopically interfering redox cofactors [109–114]. The first native Cu_A site isolated for spectroscopic and electrochemical studies was a soluble fragment from subunit II obtained from the cytochrome ba_3 oxidase from *Thermus thermophilus* (*Tt*-CuA), which contains the amino acid sequence that constitutes the Cu_A center and is highly stable at room temperature [115]. Alternatively, one of the preferred strategies to obtain stable and isolated Cu_A sites amenable to spectroscopic and electrochemical studies is the engineering of the Cu_A site into other proteins such as Azurin (Azu-Cu_A) [116–123]. In addition, the synthesis of inorganic compounds that resemble some, but not all, features of the native site has also been exploited [124–134]. Both types of artificial constructs have proven very useful in unveiling the geometric structure and some of the electronic properties of the site. On the other hand, these approaches are incomplete as very recent studies have shown that the protein scaffold plays a key role in controlling the electronic structure, and in turn, the redox properties of the site through, for example, interactions with first and second-sphere ligands [105,135–137].

The Cu_A center consists of two copper ions bridged by two cysteine ligands, forming a nearly planar Cu_2S_2 diamond core characterized by a short Cu–Cu distance (2.4 Å). The coordination sphere of the metal site is completed by two terminal histidine residues and two weakly coordinated axial ligands provided by a methionine sulfur and a backbone carbonyl (Fig. 1) [138]. Electrons shuttled by Cyt are delivered to the Cu_A site in subunit II of CcO and from there to the catalytic center embedded in subunit I, where O_2 is reduced to water. These steps involve two long, nearly perpendicular pathways through the protein milieu. Despite the low driving forces, ET takes place with high rates along these two pathways [37,139,140]. This efficiency has been attributed to the unique coordination features of Cu_A, which were suggested to yield both a low reorganization free energy and an electronic structure that enhances superexchange coupling by means of a high Cu-S_{Cys} covalency [141]. However, these features do not account for the directionality of the ET reaction while preserving quasi-reversibility.

Although the geometry and connectivity of the Cu_A site is now settled, subtleties regarding its electronic structure are currently under active discussion, as they may exert a deep impact in the redox properties of the site. In its oxidized form, Cu_A is a fully delocalized mixed-valence (MV) species ($Cu^{1.5+}$ $Cu^{1.5+}$) [142] with a σ_u^* electronic ground state (GS) [143]. Besides this electronic GS, two other alternative electronic structures have been heralded as functionally relevant, one being a localized-valence (LV) σ_u^* state and the other a MV π_u state. Here we will discuss the characteristics and physiological relevance of each state.

Lu and coworkers reported that Azu-Cu_A undergoes a pH-dependent transition to what they assigned as a LV state [144,145]. Short after, a combination of spectroscopic and theoretical methods revealed that the MV character is actually preserved in such state, except that the contribution of both Cu ions to the electronic wavefunction is asymmetric [146]. The transition to the asymmetric mixed-valence state (aMV) was shown to arise from protonation and detachment of one of the equatorial histidines resulting in a 70 mV up-shift of the redox potential and an increase in reorganization from ca. 0.4 to 0.8 eV [144,147]. Based on these results, it was hypothesized that the MV → aMV transition might regulate the functioning of CcO. Specifically, it was proposed that proton-coupled ET from the MV Cu_A site to heme *a* results in protonation of the coordinating histidine, thus inducing the MV → aMV transition that shuts down the ET activity and, thereby, interrupts proton pumping. Once the vectorial proton is released, the histidine deprotonates and the ET process is resumed [144].

Employing the native *Tt*-CuA protein fragment, we have recently shown that the MV → aMV transition does not take place in native Cu_A sites. Not only is the MV character preserved, but the equatorial histidine ligand does not detach in a pH range from 3 to 10. Moreover, the redox potential in the pH range 4–7 remains almost identical (Fig. 10) [135]. Most likely, torsional restrains and electrostatic interactions hamper the ability of native Cu_A to explore the aMV state. These results do not rule out the possibility of a pH-dependent modulation of the ET reaction in Cu_A sites that could take place through some other mechanism. However, they highlight the importance of the protein scaffolding in fine tuning the electronic and redox properties of the metal center. This was further evidenced when comparing the role of the weak axial ligand methionine in the regulation of the redox potential. Replacement of the coordinating methionine by a wide variety of amino acids did not exert any noticeable impact on the redox potential of Azu-Cu_A [148], in sharp contrast with normal azurin [149,150]. From these results it was inferred that the Cu_A site, by virtue of its structural features, is more robust to substitutions of the weak axial ligand than the T1 copper site of azurin. However, equivalent mutations of the native *Tt*-Cu_A site result in variations of the redox potential of up to 200 mV (Fig. 10) [136].

While the Cu_A center has a σ_u^* electronic GS, some inorganic model complexes have been shown to present a π_u RAMO that was postulated to represent the first excited electronic state in Cu_A sites, with an energy gap of ca. 3000 cm^{-1} as determined by EPR [151–154]. Theoretical calculations by Gorelsky and coworkers predicted that the λ values for the ET reaction of Cu_A proceeding through the π_u and σ_u^* RAMOS are 0.6 and 0.4 eV, respectively, thus rendering the π_u state thermally inaccessible and ineffective for ET [152].

Abriata and coworkers, on the other hand, determined by paramagnetic NMR that the σ_u^*/π_u energy gap is only 600 cm^{-1}, thus implying that the π_u state is in fact thermally accessible [155]. The inconsistency between paramagnetic NMR and EPR values was rationalized by Gorelsky and coworkers, based on previous theoretical work by Olsson and Ryde [152,156]. They showed that the electronic structure of the Cu_A site can be described by a double-well potential energy surface as a function of the Cu–Cu distance, with two ground states, a σ_u^* and a π_u level, with minima at ~2.4 and ~2.9 Å, respectively (Fig. 11). While the EPR experiments probe the energy associated with a vertical transition to the π_u excited electronic state, NMR experiments reveal the energy required to access the π_u state through a normal mode of vibration dominated by Cu–Cu stretching. NMR studies also revealed fast interconversion between the σ_u^* and

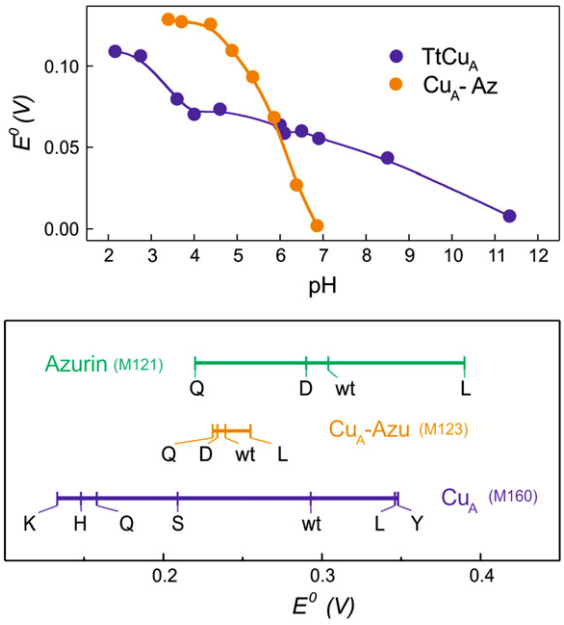

Fig. 10. Top: pH-dependencies of the redox potentials of *Tt*-Cu_A (blue) and Azu-Cu_A (orange), adapted from Alvarez-Paggi et al.[135,148] Bottom: Effect of mutation of the weak axial ligand methionine on the redox potential of *Tt*-Cu_A (blue), azurin (green) and Azu-Cu_A (orange).[136,148].

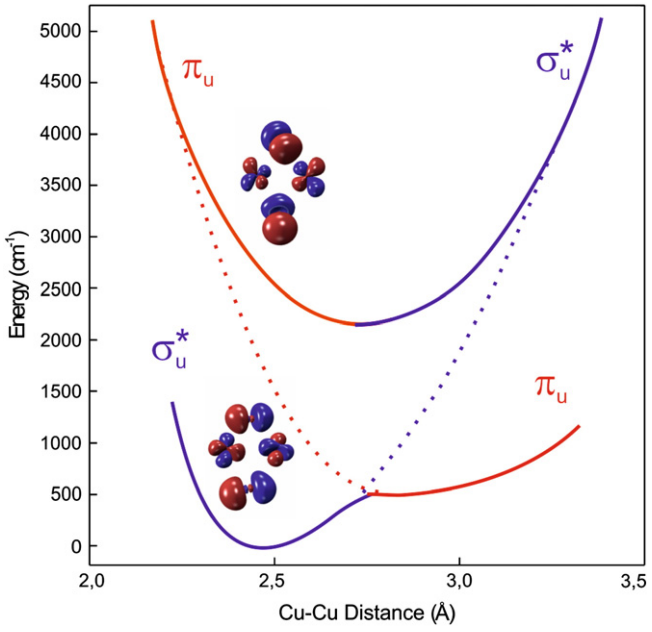

Fig. 11. Schematic potential energy surface for the Cu_A site as a function of the Cu–Cu distance, including the first excited electronic state. Elongation of the Cu–Cu distance promotes switching from the GS σ_u^* symmetry (blue) to that of π_u symmetry. Adapted from Abriata et al. [137].

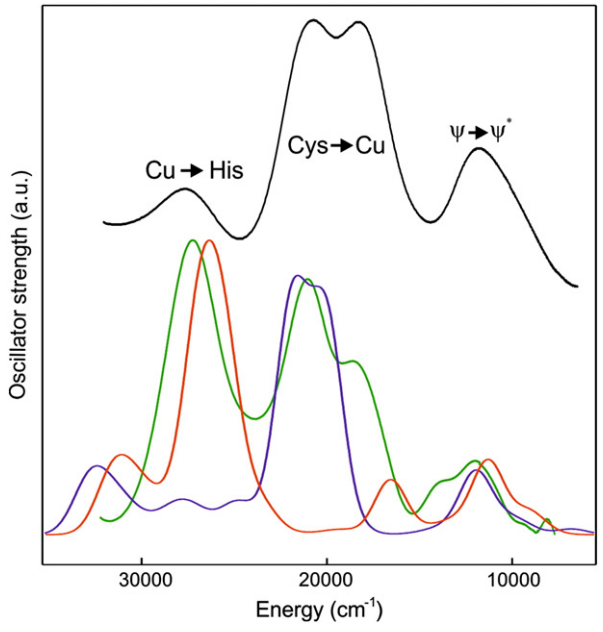

Fig. 12. Top: Experimental UV/vis spectra of *Tt*-Cu_A WT. Bottom: Experimental UV/Vis spectra of *Tt*-Cu_A M160H (green) and TD-DFT calculated UV–vis spectra of the σ_u^* and π_u. Adapted from Abriata et al. [137].

π_u ground states. Nevertheless, based on the low population of the π_u ground state at physiological temperature and on its larger λ value, it was concluded that the σ_u^* state is the only relevant RAMO [152,156].

Paramagnetic NMR studies showed that the mutations of the M160 weak axial ligand of *Tt*-Cu_A discussed previously not only changed the redox potential, but also tune the σ_u^*/π_u energy gap, thereby offering a unique opportunity to experimentally probe the redox and spectroscopic properties of the π_u state in the native protein environment [137] The absorption spectra of oxidized Cu_A centers in the σ_u^* state are dominated by two intense $S_{Cys} \rightarrow Cu$ charge transfer (CT) bands at 21,270 and 18,700 cm^{-1}, $N_{His} \rightarrow Cu$ CT transitions at 28,000 and 25,800 cm^{-1} and an intervalence band ($\psi \rightarrow \psi^*$) at 12,650 cm^{-1} that reflects the electronic coupling between the two copper ions [146,157]. The electronic spectrum of the a π_u GS, as revealed both experimentally and theoretically through TD-DFT calculations, presents a blue-shift of the $S_{Cys} \rightarrow Cu$ CT bands to ~28,000 cm^{-1} that partially overlap the $N_{His} \rightarrow Cu$ CT bands, whereas the intervalence transition appears at 12,100 cm^{-1}, thus reflecting a decrease in the Cu–Cu interaction with respect to the σ_u^* state (Fig. 12). The spectroscopic features found for the π_u state reveal that this state was actually observed in other Cu_A sites, such as the one engineered in *Escherichia coli* quinol oxidase, although it was not recognized at the time [151]. In these cases the absorption spectra of the σ_u^* and π_u states appeared convoluted, thus suggesting a role not only of the first sphere ligands but also of the protein matrix in fine tuning the σ_u^*/π_u energy gap. Following this evidence, we looked for perturbations that could result in the $\sigma_u^* \rightarrow \pi_u$ transition in the native Cu_A site, other than Cu – Cu stretching. Interestingly, we found that a large number of structural distortions, such as torsion of the histidine ligands and disruption of the planarity of the Cu_2S_2 moiety that do not imply significant Cu–Cu elongation actually drive the Cu_A site to a π_u GS [137].

Theoretical calculations performed on Azu-Cu_A predict that, due to the high covalency of the Cu_2S_2 moiety and the almost null contribution of the axial ligands to the RAMO wavefunction, the incoming and outgoing ET pathways involve the coordinating cysteines [158]. However, paramagnetic NMR determinations on *Tt*-Cu_A show that the π_u state but not the σ_u^* state presents spin density on the M160 weak axial ligand. This result prompted us to study the covalencies of both the σ_u^* and π_u state for the native *Tt*-CuA site in both redox states, and how they may affect the ET pathways. As structural model we employed the structure of the *Tt*-CuA/Cyt-c_{552} complex reported by Muresanu et al. [37]. Pathways calculations for ET from heme *c* towards the Cu_A site showed that the electronic coupling was maximized for electron entry through the weak axial ligand M160 (Fig. 13). The covalency of the S_{M160} atom increases tenfold in the π_u state compared to the σ_u^* state, which translates into a 100 times increase of the ET probability. The covalency calculation is in good agreement with the experimental observation of spin density, which implies some degree of d_{z2} mixing. Thus, these results suggest that the π_u state is optimal for accepting electrons from Cyt-c_{552} because a higher electronic coupling may (over) compensate the lower thermal population and higher reorganization energy of such state. This hypothesis is supported by results obtained for the *Tt*-Cu_A M160H mutant. For this first sphere mutant the ET reaction may proceed either through the σ_u^* or the π_u state, as we are able

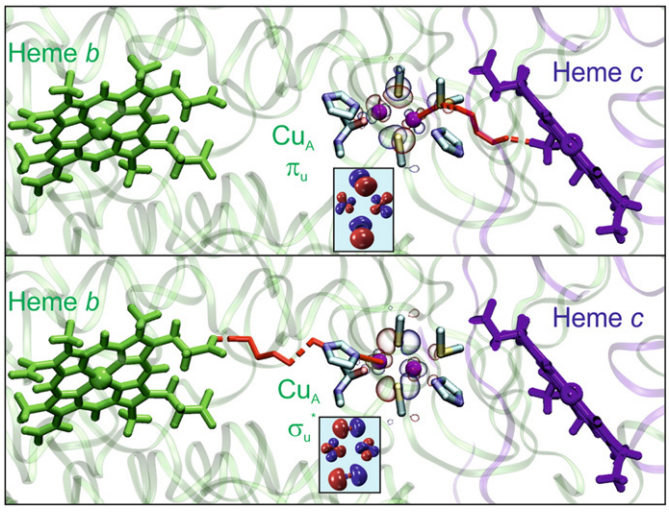

Fig. 13. Optimal electronic pathways for electron entry (top) and exit (bottom) at the Cu_A site, in the π_u and σ_u^* GS, respectively. Adapted from Abriata et al. [137].

to tune the energy gap by changing the pH of the solution. Electrochemical experiments on this protein variant yield $\lambda = 0.7$ eV for the π_u GS and $\lambda = 0.3$ eV for the σ_u^* GS. However, in spite of the higher λ value, k_{ET} is higher for the π_u state due to an enhanced electronic coupling with the metal electrode.

Pathways calculations for the ET reaction between the reduced Cu_A and heme *a* in the *ba*$_3$ oxidase from *T. thermophilus* show that the preferred exit point is through histidine 157 (Fig. 13). Calculation of the covalencies for the *Tt*-Cu_A site in the reduced state show an enhanced N_{H157}–Cu coupling in the σ_u^* state, accelerating the reaction rate by a factor of 4. Although the enhancement due to covalencies is low, this effect adds to the lower reorganization energy and higher population of the σ_u^* state, rendering it suitable for electron exit.

Thus, we propose that the Cu_A site may act as an electron hub, employing the alternative ground states to switch between electronic structures whose kinetic parameters are differentially optimized for electron entry and exit (Fig. 13).

4. Model for the regulation of the Cyt/CcO ET reaction

Direct assessment of the multiple physicochemical and structural parameters that modulate inter- and intra-protein ET reactions in real complete systems is severely hampered by the complexity of these macromolecular systems. The results presented in the preceding sections for Cyt and Cu_A sites in simplified model complexes, however, provide a unique framework for hypothesizing on how protein dynamics may affect the Cyt/CcO ET reaction *in vivo* and, moreover, on the possible existence of an electric field-driven negative feedback mechanism that may regulate electroprotonic energy transduction. This hypothesis is schematically summarized in Fig. 14.

The primary function of Cyt is shuttling electrons from complex III to complex IV. In the meantime, spurious ET reactions with other redox active molecules should be suppressed or slowed down, which could be achieved by Cyt residing in a high λ conformation that is characterized by a preserved Met80/Y67 H-bonding interaction. Recognition and binding of Cyt to CcO requires electrostatic interactions between surface lysines of Cyt and negatively charged residues in the CcO binding site. The initial recognition and complex formation does not necessarily lead to an optimized electron pathway between heme *c* and the Cu_A acceptor, thus requiring reorientation of Cyt in the complex to enhance H_{DA}. The electrostatic contacts may induce distortions of the protein matrix which ultimately lead to the interruption of the Met80/Y67 H-bond and the concomitant conversion of Cyt to its low λ native conformation.

The Cu_A site, in its idle state, resides mainly in the σ_u^* state, but it may be driven into the π_u GS by structural perturbations that take place during complex formation. Examples of copper sites undergoing structural deformations upon interactions with their redox partners include the complexes rusticyanin/Cyt-c_4, plastocyanin/Cyt-*f* and plastocyanin/photosystem I, in which both the geometric structures and the electronic densities of the copper sites are affected [159,160]. Even more relevant for our discussion, NMR studies have evidenced small structural perturbations in the Cyt-c_{552}/Cu_A complex [37]. Thus, achievement of a fully reactive complex could involve distortion of the Cu_A site, leading to a π_u GS that enhances H_{DA} with the heme *c*. It should be stressed that the enhanced H_{DA} alone should be sufficient for the ET reaction to proceed through the π_u GS because of the fast interconversion between both GS and the thermal accessibility of the π_u state even in the absence of external perturbations. After the Cu_A site is reduced, the lower reorganization energy of the σ_u^* GS together with the enhanced H_{DA} with heme *a* prompt the redox ET to proceed, thus conferring directionality to the overall process in spite of the very low thermodynamic driving forces.

The studies on model complexes suggest that the system admits many possible control points. Local electric fields are the result of transmembrane, dipole and surface potentials that arise from the global balance of proton pumping activity by all respiratory complexes in the membrane and its consumption by ATP synthases. A temporary misbalance in proton pumping/consumption may result in increased local electric fields that may slow down Cyt reorientation, thus undermining its ability to achieve orientations that correspond to high H_{DA} with the Cu_A electron acceptor. In addition, the theoretical calculations predict that the σ_u^*/π_u energy gap increases with increasing electric fields, thus reducing the probability of populating the π_u state [137]. Therefore, the increase of the local electric field is expected to temporarily block or significantly slow down the PCET reactions of the Cyt/CcO complex, until the proton electrochemical gradient is sufficiently dissipated by translocation *via* the ATP-synthase.

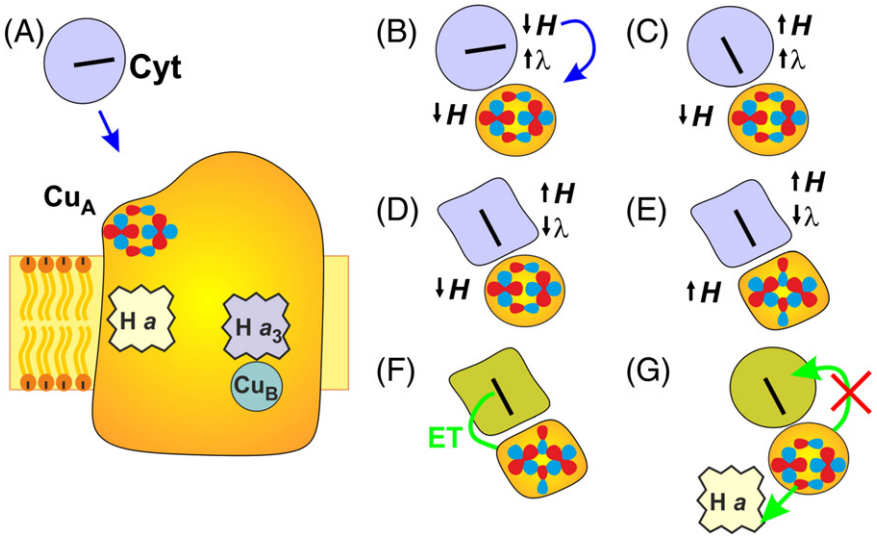

Fig. 14. Schematic representation of the regulatory model for the Cyt/CcO ET reaction. Cyt shuttles an electron towards the CcO, and docks near the Cu_A site (A). The complex is not optimized for ET so Cyt must reorient (B) in order to achieve a higher electronic coupling (C). In the process, more Cyt/CcO contacts are established, triggering a conformational transition of Cyt towards a lower λ form (D). The Cu_A site is perturbed in such a way that the π_u GS may be favored, thus further optimizing the electronic coupling (E). The ET reaction is then kinetically favored in spite of the low driving force and proceeds (F). Directionality is preserved and back ET is hampered because after the ET reaction the features that optimize the reaction are lost, and so the intramolecular ET towards Heme *a* proceeds (G). Steps (B), (D) and (E) may be negatively affected by the strength of the interfacial electric field that increases because of the proton pumping resulting from the ET reactions. Thus, a regulatory negative feedback may be established due to the interplay between electron and proton transfer reactions. When the electric field lowers due to the activity of the ATP synthase the ET activity may be resumed.

Even higher electric fields have been shown to induce structural changes of Cyt that result in the gain of peroxidatic activity of potential relevance in the early events of apoptosis [58,59,161,162].

5. Conclusions

The notion of a "native" state associated with protein function is not sufficient for successfully describing intra- and inter-protein ET reactions. We have shown that protein dynamics and thermal fluctuations allow these systems to explore different structural and electronic configurations that are crucial for their function, optimizing the kinetic parameters in different ways. Moreover, electrostatic interactions and local electric fields reshape the free energy surfaces that the proteins explore, in a manner that may be central for regulation of the respiratory electron transport chain, as well as other systems unrelated to the respiratory function. Although these proposals are yet to be tested in reactive complexes *in vivo*, the physicochemical studies on model systems presented here enabled us to obtain a detailed molecular picture of possible regulatory mechanisms, thus paving the way for future investigations.

Acknowledgments

Financial support from the ANPCyT (PICT2010-70 and PICT2011-1249) and from UBACyT is gratefully acknowledged. DAP and UZ thank CONICET for fellowships. DHM is member of CONICET. This research was done using the resources provided by the Open Science Grid, which is supported by the National Science Foundation and the U.S. Department of Energy's Office of Science.

References

[1] X. Zhuang, et al., Correlating structural dynamics and function in single ribozyme molecules, Science 296 (5572) (2002) 1473–1476.
[2] D.E. Shaw, et al., Atomic-level characterization of the structural dynamics of proteins, Science 330 (6002) (2010) 341–346.
[3] H. Frauenfelder, et al., A unified model of protein dynamics, Proc. Natl. Acad. Sci. U. S. A. 106 (13) (2009) 5129–5134.
[4] Q. Bashir, S. Scanu, M. Ubbink, Dynamics in electron transfer protein complexes, FEBS J. 278 (9) (2011) 1391–1400.
[5] K.K. Chohan, et al., Protein dynamics enhance electronic coupling in electron transfer complexes, J. Biol. Chem. 276 (36) (2001) 34142–34147.
[6] J.N. Gehlen, M. Marchi, D. Chandler, Dynamics affecting the primary charge transfer in photosynthesis, Science 263 (5146) (1994) 499–501.
[7] P. Kundu, A. Dua, Protein dynamics modulated electron transfer kinetics in early stage photosynthesis, J. Chem. Phys. 138 (4) (2013) 045104.
[8] T.R. Prytkova, I.V. Kurnikov, D.N. Beratan, Coupling coherence distinguishes structure sensitivity in protein electron transfer, Science 315 (5812) (2007) 622–625.
[9] S.S. Skourtis, I.A. Balabin, T. Kawatsu, D.N. Beratan, Protein dynamics and electron transfer: electronic decoherence and non-Condon effects, Proc. Natl. Acad. Sci. U. S. A. 102 (10) (2005) 3552–3557.
[10] H. Sumi, R.A. Marcus, Dynamical effects in electron transfer reactions, J. Chem. Phys. 84 (1986) 4894.
[11] M.L. Tan, I. Balabin, J.N. Onuchic, Dynamics of electron transfer pathways in cytochrome *c* oxidase, Biophys. J. 86 (3) (2004) 1813–1819.
[12] H. Wang, et al., Protein dynamics control the kinetics of initial electron transfer in photosynthesis, Science 316 (5825) (2007) 747–750.
[13] H. Wang, Y. Hao, Y. Jiang, S. Lin, N.W. Woodbury, Role of protein dynamics in guiding electron-transfer pathways in reaction centers from *Rhodobacter sphaeroides*, J. Phys. Chem. B 116 (1) (2011) 711–717.
[14] K.E. Wheeler, et al., Dynamic docking of cytochrome b_5 with myoglobin and α-hemoglobin: heme-neutralization "squares" and the binding of electron-transfer-reactive configurations, J. Am. Chem. Soc. 129 (13) (2007) 3906–3917.
[15] A.V. Zhuravleva, et al., Gated electron transfers and electron pathways in azurin: a NMR dynamic study at multiple fields and temperatures, J. Mol. Biol. 342 (5) (2004) 1599–1611.
[16] A. Kranich, H.K. Ly, P. Hildebrandt, D.H. Murgida, Direct observation of the gating step in protein electron transfer: electric-field-controlled protein dynamics, J. Am. Chem. Soc. 130 (30) (2008) 9844–9848.
[17] G.W. Bushnell, G.V. Louie, G.D. Brayer, High-resolution three-dimensional structure of horse heart cytochrome *c*, J. Mol. Biol. 214 (2) (1990) 585–595.
[18] P.A. Williams, et al., The CuA domain of Thermus thermophilus ba3-type cytochrome c oxidase at 1.6 Å resolution, Nat. Struct. Mol. Biol. 6 (6) (1999) 509–516.
[19] R.A. Marcus, Chemical and electrochemical electron-transfer theory, Annu. Rev. Phys. Chem. 15 (1) (1964) 155–196.
[20] R.A. Marcus, Electron transfer reactions in chemistry: theory and experiment (Nobel lecture), Angew. Chem. Int. Edit. 32 (8) (1993) 1111–1121.
[21] R.R. Dogonadze, A.M. Kuznetsov, A.A. Chernenko, Theory of homogeneous and heterogeneous electronic processes in liquids, Russ. Chem. Rev. 34 (1965) 759–775.
[22] W.R. Fawcett, M. Opallo, The kinetics of heterogeneous electron transfer reaction in polar solvents, Angew. Chem. Int. Edit. 33 (21) (1994) 2131–2143.
[23] R.K. Sen, E. Yeager, W.E. O'Grady, Theory of charge transfer at electrochemical interfaces, Annu. Rev. Phys. Chem. 26 (1) (1975) 287–314.
[24] A.M. Kuznetsov, J. Ulstrup, Theory of electron transfer at electrified interfaces, Electrochim. Acta 45 (15–16) (2000) 2339–2361.
[25] J. Ulstrup, J. Jortner, The effect of intramolecular quantum modes on free energy relationships for electron transfer reactions, J. Chem. Phys. 63 (10) (1975) 4358–4368.
[26] N.S. Hush, Adiabatic theory of outer sphere electron-transfer reactions in solution, Trans. Faraday Soc. 57 (1961) 557–580.
[27] J.J. Hopfield, Electron transfer between biological molecules by thermally activated tunneling, Proc. Natl. Acad. Sci. U. S. A. 71 (9) (1974) 3640.
[28] J.N. Betts, D.N. Beratan, J.N. Onuchic, Mapping electron tunneling pathways: an algorithm that finds the "minimum length"/maximum coupling pathway between electron donors and acceptors in proteins, J. Am. Chem. Soc. 114 (11) (1992) 4043–4046.
[29] S.S. Skourtis, D.H. Waldeck, D.N. Beratan, Fluctuations in biological and bioinspired electron-transfer reactions, Annu. Rev. Phys. Chem. 61 (2010) 461–485.
[30] I.A. Balabin, D.N. Beratan, S.S. Skourtis, Persistence of structure over fluctuations in biological electron-transfer reactions, Phys. Rev. Lett. 101 (15) (2008) 158102–158106.
[31] D.N. Beratan, J.N. Betts, J.N. Onuchic, Protein electron transfer rates set by the bridging secondary and tertiary structure, Science 252 (5010) (1991) 1285–1288.
[32] M. Hervás, M.A. Rosa, G. Tollin, A comparative laser-flash absorption spectroscopy study of algal plastocyanin and cytochrome c_{552} photooxidation by photosystem I particles from spinach, Eur. J. Biochem. 203 (1–2) (1992) 115–120.
[33] J.T. Hazzard, S.Y. Rong, G. Tollin, Ionic strength dependence of the kinetics of electron transfer from bovine mitochondrial cytochrome *c* to bovine cytochrome *c* oxidase, Biochemistry 30 (1) (1991) 213–222.
[34] M. Ubbink, M. Ejdebäck, B.G. Karlsson, D.S. Bendall, The structure of the complex of plastocyanin and cytochrome *f*, determined by paramagnetic NMR and restrained rigid-body molecular dynamics, Structure 6 (3) (1998) 323–335.
[35] P.B. Crowley, M. Ubbink, Close encounters of the transient kind: protein interactions in the photosynthetic redox chain investigated by NMR spectroscopy, Acc. Chem. Res. 36 (10) (2003) 723–730.
[36] A.N. Volkov, J.A. Worrall, E. Holtzmann, M. Ubbink, Solution structure and dynamics of the complex between cytochrome c and cytochrome c peroxidase determined by paramagnetic NMR, Proc. Natl. Acad. Sci. U. S. A. 103 (50) (2006) 18945–18950.
[37] L. Muresanu, et al., The electron transfer complex between cytochrome c_{552} and the Cu_A domain of the *Thermus thermophilus* ba_3 oxidase, J. Biol. Chem. 281 (20) (2006) 14503–14513.
[38] K.L. Prime, G.M. Whitesides, Self-assembled organic monolayers: model systems for studying adsorption of proteins at surfaces, Science 252 (5010) (1991) 1164–1167.
[39] D. Samanta, A. Sarkar, Immobilization of bio-macromolecules on self-assembled monolayers: methods and sensor applications, Chem. Soc. Rev. 40 (5) (2011) 2567–2592.
[40] S.K. Arya, P.R. Solanki, M. Datta, B.D. Malhotra, Recent advances in self-assembled monolayers based biomolecular electronic devices, Biosens. Bioelectron. 24 (9) (2009) 2810–2817.
[41] C.E. Chidsey, Free energy and temperature dependence of electron transfer at the metal-electrolyte interface, Science 251 (4996) (1991) 919–922.
[42] H.M. McConnell, Intramolecular charge transfer in aromatic free radicals, J. Chem. Phys. 35 (1961) 508–515.
[43] C.A. Naleway, L.A. Curtiss, J.R. Miller, Superexchange-pathway model for long-distance electronic couplings, J. Phys. Chem. 95 (22) (1991) 8434–8437.
[44] A. Avila, B.W. Gregory, K. Niki, T.M. Cotton, An electrochemical approach to investigate gated electron transfer using a physiological model system: cytochrome *c* immobilized on carboxylic acid-terminated alkanethiol self-assembled monolayers on gold electrodes, J. Phys. Chem. B 104 (12) (2000) 2759–2766.
[45] Q.J. Chi, J.D. Zhang, J.E.T. Andersen, J. Ulstrup, Ordered assembly and controlled electron transfer of the blue copper protein azurin at gold (111) single-crystal substrates, J. Phys. Chem. B 105 (20) (2001) 4669–4679.
[46] K.L. Davis, D.H. Waldeck, Effect of deuterium substitution on electron transfer at cytochrome OSAM interfaces, J. Phys. Chem. B 112 (39) (2008) 12498–12507.
[47] A. El Kasmi, J.M. Wallace, E.F. Bowden, S.M. Binet, R.J. Linderman, Controlling interfacial electron-transfer kinetics of cytochrome *c* with mixed self-assembled monolayers, J. Am. Chem. Soc. 120 (1) (1998) 225–226.
[48] J.J. Feng, et al., Gated electron transfer of yeast iso-1 cytochrome c on SAM-coated electrodes, J. Phys. Chem. B 112 (2008) 15202–15211.
[49] A. Kranich, et al., Gated electron transfer of cytochrome c_6 at biomimetic interfaces: a time-resolved SERR study, Phys. Chem. Chem. Phys. 11 (34) (2009) 7390–7397.
[50] M.F. Molinas, et al., Electron transfer dynamics of *Rhodothermus marinus* caa_3 cytochrome *c* domains on biomimetic films, Phys. Chem. Chem. Phys. 13 (40) (2011) 18088–18098.
[51] D.H. Murgida, P. Hildebrandt, Proton-coupled electron transfer of cytochrome *c*, J. Am. Chem. Soc. 123 (17) (2001) 4062–4068.

[52] K. Niki, et al., Coupling to lysine-13 promotes electron tunneling through carboxylate-terminated alkanethiol self-assembled monolayers to cytochrome c, J. Phys. Chem. B 107 (37) (2003) 9947–9949.
[53] J.J. Wei, et al., Electron-transfer dynamics of cytochrome C: a change in the reaction mechanism with distance, Angew. Chem. Int. Ed. 41 (24) (2002) 4700–4703.
[54] J.S. Xu, E.F. Bowden, Determination of the orientation of adsorbed cytochrome *c* on carboxyalkanethiol self-assembled monolayers by in situ differential modification, J. Am. Chem. Soc. 128 (21) (2006) 6813–6822.
[55] H.J. Yue, et al., On the electron transfer mechanism between cytochrome c and metal electrodes. Evidence for dynamic control at short distances, J. Phys. Chem. B 110 (40) (2006) 19906–19913.
[56] P. Zuo, T. Albrecht, P.D. Barker, D.H. Murgida, P. Hildebrandt, Interfacial redox processes of cytochrome b_{562}, Phys. Chem. Chem. Phys. 11 (34) (2009) 7430–7436.
[57] K. Fujita, et al., Mimicking protein–protein electron transfer: voltammetry of *Pseudomonas aeruginosa* azurin and the *Thermus thermophilus* Cu_A domain at ω-derivatized self-assembled-monolayer gold electrodes, J. Am. Chem. Soc. 126 (43) (2004) 13954–13961.
[58] D.H. Murgida, P. Hildebrandt, Heterogeneous electron transfer of cytochrome c on coated silver electrodes. Electric field effects on structure and redox potential, J. Phys. Chem. B 105 (8) (2001) 1578–1586.
[59] D.H. Murgida, P. Hildebrandt, Electron-transfer processes of cytochrome *c* at interfaces. New insights by surface-enhanced resonance Raman spectroscopy, Acc. Chem. Res. 37 (11) (2004) 854–861.
[60] D.H. Murgida, P. Hildebrandt, Disentangling interfacial redox processes of proteins by SERR spectroscopy, Chem. Soc. Rev. 37 (5) (2008) 937–945.
[61] M. Moskovits, J.S. Suh, Surface selection rules for surface-enhanced Raman spectroscopy: calculations and application to the surface-enhanced Raman spectrum of phthalazine on silver, J. Phys. Chem. 88 (23) (1984) 5526–5530.
[62] H. Wackerbarth, U. Klar, W. Gunther, P. Hildebrandt, Novel time-resolved surface-enhanced (resonance) Raman spectroscopic technique for studying the dynamics of interfacial processes: application to the electron transfer reaction of cytochrome *c* at a silver electrode, Appl. Spectrosc. 53 (3) (1999) 283–291.
[63] D. Alvarez-Paggi, et al., Molecular basis of coupled protein and electron transfer dynamics of cytochrome *c* in biomimetic complexes, J. Am. Chem. Soc. 132 (16) (2010) 5769–5778.
[64] H.K. Ly, et al., Thermal fluctuations determine the electron-transfer rates of cytochrome *c* in electrostatic and covalent complexes, ChemPhysChem 11 (6) (2010) 1225–1235.
[65] D.A. Paggi, et al., Computer simulation and SERR detection of cytochrome *c* dynamics at SAM-coated electrodes, Electrochim. Acta 54 (22) (2009) 4963–4970.
[66] W.H. Koppenol, J.D. Rush, J.D. Mills, E. Margoliash, The dipole-moment of cytochrome-C, Mol. Biol. Evol. 8 (4) (1991) 545–558.
[67] R.J. Clarke, The dipole potential of phospholipid membranes and methods for its detection, Adv. Colloid Interfac. 89 (2001) 263–281.
[68] C.P. Smith, H.S. DWhite, Theory of the interfacial potential distribution and reversible voltammetric response of electrodes coated with electroactive molecular films, Anal. Chem. 64 (20) (1992) 2398–2405.
[69] H. Pelletier, J. Kraut, Crystal structure of a complex between electron transfer partners, cytochrome *c* peroxidase and cytochrome *c*, Science 258 (5089) (1992) 1748–1755.
[70] C. Lange, C. Hunte, Crystal structure of the yeast cytochrome bc_1 complex with its bound substrate cytochrome *c*, Proc. Natl. Acad. Sci. U. S. A. 99 (5) (2002) 2800–2805.
[71] V.A. Roberts, M.E. Pique, Definition of the interaction domain for cytochrome *c* on cytochrome *c* oxidase, J. Biol. Chem. 274 (53) (1999) 38051–38060.
[72] J.N. Onuchic, D.N. Beratan, J.R. Winkler, H.B. Gray, Pathway analysis of protein electron-transfer reactions, Annu. Rev. Bioph. Biom. 21 (1) (1992) 349–377.
[73] D.N. Beratan, J.N. Onuchic, J.R. Winkler, H.B. Gray, Electron-tunneling pathways in proteins, Science 258 (5089) (1992) 1740–1741.
[74] D. Alvarez-Paggi, et al., Disentangling electron tunneling and protein dynamics of cytochrome c through a rationally designed surface mutation, J. Phys. Chem. B 117 (20) (2013) 6061–6068.
[75] R.A. Marcus, On the theory of oxidation-reduction reactions involving electron transfer. I, J. Chem. Phys. 24 (5) (1956) 966–978.
[76] E. Babini, et al., Bond-mediated electron tunneling in ruthenium-modified high-potential iron-sulfur protein, J. Am. Chem. Soc. 122 (18) (2000) 4532–4533.
[77] O. Miyashita, M.Y. Okamura, J.N. Onuchic, Theoretical understanding of the interprotein electron transfer between cytochrome c2 and the photosynthetic reaction center, J. Phys. Chem. B 107 (5) (2003) 1230–1241.
[78] J.R. Winkler, P. Wittung-Stafshede, J. Leckner, B.G. Malmström, H.B. Gray, Effects of folding on metalloprotein active sites, Proc. Natl. Acad. Sci. U. S. A. 94 (9) (1997) 4246–4249.
[79] R. Huber, E. Antonini plenary lecture A structural basis of light energy and electron transfer in biology, *EJB Reviews 1990*, Springer, 1991. 25–47.
[80] K.M. Lancaster, et al., Electron transfer reactivity of type zero *Pseudomonas aeruginosa* azurin, J. Am. Chem. Soc. 133 (13) (2011) 4865–4873.
[81] V. Tipmanee, H. Oberhofer, M. Park, K.S. Kim, J. Blumberger, Prediction of reorganization free energies for biological electron transfer: a comparative study of Ru-modified cytochromes and a 4-helix bundle protein, J. Am. Chem. Soc. 132 (47) (2010) 17032–17040.
[82] E. Sigfridsson, M.H.M. Olsson, U. Ryde, A comparison of the inner-sphere reorganization energies of cytochromes, iron–sulfur clusters, and blue copper proteins, J. Phys. Chem. B 105 (23) (2001) 5546–5552.
[83] C.A. Bortolotti, et al., The reorganization energy in cytochrome *c* is controlled by the accessibility of the heme to the solvent, J. Phys. Chem. Lett. 2 (14) (2011) 1761–1765.
[84] I. Muegge, P.X. Qi, A.J. Wand, Z.T. Chu, A. Warshel, The reorganization energy of cytochrome c revisited, J. Phys. Chem. B 101 (5) (1997) 825–836.
[85] A. Jasaitis, M.P. Johansson, M. Wikström, M.H. Vos, M.I. Verkhovsky, Nanosecond electron tunneling between the hemes in cytochrome bo_3, Proc. Natl. Acad. Sci. U. S. A. 104 (52) (2007) 20811–20814.
[86] Y.C. Kim, M. Wikström, G. Hummer, Kinetic gating of the proton pump in cytochrome *c* oxidase, Proc. Natl. Acad. Sci. U. S. A. 106 (33) (2009) 13707–13712.
[87] S.M. Andrew, K.A. Thomasson, S.H. Northrup, Simulation of electron-transfer self-exchange in cytochrome *c* and cytochrome b_5, J. Am. Chem. Soc. 115 (13) (1993) 5516–5521.
[88] T.D. Dolidze, S. Rondinini, A. Verto-Va, D.H. Waldeck, D.E. Khoshtariya, Impact of self-assembly composition on the alternate interfacial electron transfer for electrostatically immobilized cytochrome *c*, Biopolymers 87 (1) (2007) 68–73.
[89] M. Fedurco, et al., Electrochemistry of unfolded cytochrome *c* in neutral and acidic urea solutions, J. Am. Chem. Soc. 127 (20) (2005) 7638–7646.
[90] H.B. Gray, J.R. Winkler, Electron tunneling through proteins, Q. Rev. Biophys. 36 (3) (2003) 341–372.
[91] T.M. Nahir, R.A. Clark, E.F. Bowden, Linear-sweep voltammetry of irreversible electron-transfer in surface-confined species using the Marcus theory, Anal. Chem. 66 (15) (1994) 2595–2598.
[92] H. Shafiey, H. Ghourchian, N. Mogharrab, How does reorganization energy change upon protein unfolding? Monitoring the structural perturbations in the heme cavity of cytochrome *c*, Biophys. Chem. 134 (3) (2008) 225–231.
[93] S. Song, R.A. Clark, E.F. Bowden, M.J. Tarlov, Characterization of cytochrome *c* alkanethiolate structures prepared by self-assembly on gold, J. Phys. Chem. 97 (24) (1993) 6564–6572.
[94] S. Terrettaz, J. Cheng, C.J. Miller, Kinetic parameters for cytochrome *c* via insulated electrode voltammetry, J. Am. Chem. Soc. 118 (33) (1996) 7857–7858.
[95] D.V. Matyushov, Nanosecond stokes shift dynamics, dynamical transition, and gigantic reorganization energy of hydrated heme proteins, J. Phys. Chem. B 115 (36) (2011) 10715–10724.
[96] H.B. Gray, J.R. Winkler, Electron transfer in proteins, Annu. Rev. Biochem. 65 (1996) 537–561.
[97] T. Ying, et al., Tyrosine-67 in cytochrome *c* is a possible apoptotic trigger controlled by hydrogen bonds via a conformational transition, Chem. Commun. 30 (2009) 4512–4514.
[98] L.A. Abriata, et al., Nitration of solvent-exposed tyrosine 74 on cytochrome *c* triggers heme iron-methionine 80 bond disruption, J. Biol. Chem. 284 (1) (2009) 17–26.
[99] A.M. Berghuis, et al., The role of a conserved internal water molecule and its associated hydrogen bond network in cytochrome *c*, J. Mol. Biol. 236 (3) (1994) 786–799.
[100] T.L. Luntz, A. Schejter, E.A. Garber, E. Margoliash, Structural significance of an internal water molecule studied by site-directed mutagenesis of tyrosine-67 in rat cytochrome *c*, Proc. Natl. Acad. Sci. U. S. A. 86 (10) (1989) 3524–3528.
[101] B.A. Feinberg, L. Petro, G. Hock, Q. Wenying, E. Margoliash, Using entropies of reaction to predict changes in protein stability: tyrosine-67-phenylalanine variants of rat cytochrome *c* and yeast iso-1 cytochromes *c*, J. Pharm. Biomed. Anal. 19 (1–2) (1999) 115–125.
[102] G. Battistuzzi, et al., Role of Met80 and Tyr67 in the low-pH conformational equilibria of cytochrome *c*, Biochemistry 51 (30) (2012) 5967–5978.
[103] J.M. García-Heredia, et al., Nitration of tyrosine 74 prevents human cytochrome *c* to play a key role in apoptosis signaling by blocking caspase-9 activation, BBA-Bioenergetics 1797 (6) (2010) 981–993.
[104] P. Zhou, F. Tian, F. Lv, Z. Shang, Geometric characteristics of hydrogen bonds involving sulfur atoms in proteins, Proteins Struct. Funct. Bioinf. 76 (1) (2009) 151–163.
[105] D. Alvarez-Paggi, et al., Electrostatically driven second-sphere ligand switch between high and low reorganization energy forms of native cytochrome *c*, J. Am. Chem. Soc. 135 (11) (2013) 4389–4397.
[106] O. Kokhan, C.A. Wraight, E. Tajkhorshid, The binding interface of cytochrome *c* and cytochrome c_1 in the bc_1 complex: rationalizing the role of key residues, Biophys. J. 99 (8) (2010) 2647–2656.
[107] S.J. Takayama, et al., Electron transfer from cytochrome *c* to cupredoxins, J. Biol. Inorg. Chem. 14 (6) (2009) 821–828.
[108] H. Beinert, Copper A of cytochrome *c* oxidase, a novel, long-embattled, biological electron-transfer site, Eur. J. Biochem. 245 (3) (1997) 521–532.
[109] K. Brown, et al., A novel type of catalytic copper cluster in nitrous oxide reductase, Nat. Struct. Mol. Biol. 7 (3) (2000) 191–195.
[110] T. Haltia, et al., Crystal structure of nitrous oxide reductase from *Paracoccus denitrificans* at 1.6 Å resolution, Biochem. J. 369 (Pt 1) (2003) 77.
[111] G.T. Babcock, M. Wikström, Oxygen activation and the conservation of energy in cell respiration, Nature 356 (6367) (1992) 301–309.
[112] M. Wikström, Cytochrome *c* oxidase: 25 years of the elusive proton pump, BBA-Bioenergetics 1655 (1–3) (2004) 241–247.
[113] T. Tsukihara, et al., Structures of metal sites of oxidized bovine heart cytochrome *c* oxidase at 2.8 Å, Science 269 (5227) (1995) 1069–1074.
[114] S. Iwata, C. Ostermeier, B. Ludwig, H. Michel, Structure at 2.8 Å resolution of cytochrome *c* oxidase from *Paracoccus denitrificans*, Nature 376 (6542) (1995) 660–668.
[115] C.E. Slutter, et al., Water-soluble, recombinant Cu_A-domain of the cytochrome ba_3 subunit II from *Thermus thermophilus*, Biochemistry 35 (11) (1996) 3387–3395.
[116] J. van der Oost, et al., Restoration of a lost metal-binding site: construction of two different copper sites into a subunit of the *E. coli* cytochrome o quinol oxidase complex, EMBO J. 11 (9) (1992) 3209.

[117] C. Dennison, E. Vijgenboom, S. de Vries, J. van der Oost, G.W. Canters, Introduction of a Cu_A site into the blue copper protein amicyanin from *Thiobacillus versutus*, FEBS Lett. 365 (1) (1995) 92–94.

[118] M. Wilmanns, P. Lappalainen, M. Kelly, E. Sauer-Eriksson, M. Saraste, Crystal structure of the membrane-exposed domain from a respiratory quinol oxidase complex with an engineered dinuclear copper center, Proc. Natl. Acad. Sci. U. S. A. 92 (26) (1995) 11955.

[119] A. Uchida, T. Kusano, T. Mogi, Y. Anraku, N. Sone, Expression of the *Escherichia coli* bo-type ubiquinol oxidase with a chimeric subunit ii having the Cu_A-Cytochrome *c* domain from the *Thermophilic Bacillus caa*$_3$-type cytochrome *c* oxidase, J. Biochem. 122 (5) (1997) 1004–1009.

[120] C. Dennison, E. Vijgenboom, W.R. Hagen, G.W. Canters, Loop-directed mutagenesis converts amicyanin from *Thiobacillus versutus* into a novel blue copper protein, J. Am. Chem. Soc. 118 (31) (1996) 7406–7407.

[121] L.H. Jones, A. Liu, V.L. Davidson, An engineered Cu_A amicyanin capable of intermolecular electron transfer reactions, J. Biol. Chem. 278 (47) (2003) 47269–47274.

[122] M. Hay, J.H. Richards, Y. Lu, Construction and characterization of an azurin analog for the purple copper site in cytochrome c oxidase, Proc. Natl. Acad. Sci. U. S. A. 93 (1) (1996) 461.

[123] M.T. Hay, et al., Spectroscopic characterization of an engineered purple Cu_A center in azurin, Inorg. Chem. 37 (2) (1998) 191–198.

[124] S.B. Harkins, J.C. Peters, Amido-bridged Cu2N2 diamond cores that minimize structural reorganization and facilitate reversible redox behavior between a Cu1Cu1 and a class III delocalized Cu1. 5Cu1. 5 species, J. Am. Chem. Soc. 126 (9) (2004) 2885–2893.

[125] C. He, S.J. Lippard, Synthesis and characterization of several dicopper (I) complexes and a spin-delocalized dicopper (I, II) mixed-valence complex using a 1, 8-naphthyridine-based dinucleating ligand, Inorg. Chem. 39 (23) (2000) 5225–5231.

[126] R. Gupta, Z.H. Zhang, D. Powell, M.P. Hendrich, A.S. Borovik, Synthesis and characterization of completely delocalized mixed-valent dicopper complexes, Inorg. Chem. 41 (20) (2002) 5100–5106.

[127] M.G. Savelieff, Y. Lu, pH dependent copper binding properties of a Cu_A azurin variant with both bridging cysteines replaced with serines, Inorg. Chim. Acta 361 (4) (2008) 1087–1094.

[128] C. Harding, V. McKee, J. Nelson, Highly delocalized Cu (I)/Cu (II); a copper– copper bond? J. Am. Chem. Soc. 113 (25) (1991) 9684–9685.

[129] M.E. Barr, P.H. Smith, W.E. Antholine, B. Spencer, Crystallographic, spectroscopic and theoretical studies of an electron-deiocalized Cu (1.5)–Cu (1.5) complex, J. Chem. Soc. Chem. Commun. 21 (1993) 1649–1652.

[130] J.A. Farrar, et al., Spectroscopic studies on the average-valence copper site Cu23+, Inorg. Chem. 34 (6) (1995) 1302–1303.

[131] J.A. Farrar, R. Grinter, F. Neese, J. Nelson, A.J. Thomson, The electronic structure of the mixed-valence copper dimer [Cu2{N (CH2CH2N = CHCH = NCH2CH2)3 N}] 3+, J. Chem. Soc. Dalton (1997) 4083–4088.

[132] A. Al-Obaidi, et al., Raman spectroscopy of three average-valence dicopper cryptates: evidence for copper– copper bonding, Inorg. Chem. 37 (14) (1998) 3567–3574.

[133] R.P. Houser, J.A. Halfen, V.G. Young Jr., N.J. Blackburn, W.B. Tolman, Structural characterization of the first example of a bis (μ-thiolato) dicopper (II) complex. Relevance to proposals for the electron transfer sites in cytochrome c oxidase and nitrous oxide reductase, J. Am. Chem. Soc. 117 (43) (1995) 10745–10746.

[134] R.P. Houser, V.G. Young Jr., W.B. Tolman, A thiolate-bridged, fully delocalized mixed-valence dicopper (I, II) complex that models the Cu_A biological electron-transfer site, J. Am. Chem. Soc. 118 (8) (1996) 2101–2102.

[135] D. Alvarez-Paggi, L.A. Abriata, D.H. Murgida, A.J. Vila, Native Cu_A redox sites are largely resilient to pH variations within physiological range, Chem. Commun. 49 (47) (2013) 5381–5383.

[136] G.N. Ledesma, et al., The met axial ligand determines the redox potential in cu_a sites, J. Am. Chem. Soc. 129 (39) (2007) 11884–11885.

[137] L.A. Abriata, et al., Alternative ground states enable pathway switching in biological electron transfer, Proc. Natl. Acad. Sci. 109 (43) (2012) 17348–17353.

[138] B.E. Ramirez, B.G. Malmström, J.R. Winkler, H.B. Gray, The currents of life: the terminal electron-transfer complex of respiration, Proc. Natl. Acad. Sci. U. S. A. 92 (26) (1995) 11949.

[139] O. Farver, Y. Chen, J.A. Fee, I. Pecht, Electron transfer among the Cu_A-, heme *b*-and a_3-centers of *Thermus thermophilus* cytochrome ba_3, FEBS Lett. 580 (14) (2006) 3417–3421.

[140] P. Brzezinski, Internal electron-transfer reactions in cytochrome *c* oxidase, Biochemistry 35 (18) (1996) 5611–5615.

[141] D.W. Randall, D.R. Gamelin, L.B. LaCroix, E.I. Solomon, Electronic structure contributions to electron transfer in blue Cu and Cu_A, J. Biol. Inorg. Chem. 5 (1) (2000) 16–29.

[142] I. Bertini, et al., The Cu_A center of a soluble domain from *Thermus* cytochrome ba_3. An NMR investigation of the paramagnetic protein, J. Am. Chem. Soc. 118 (46) (1996) 11658–11659.

[143] P.M.H. Kroneck, et al., Multifrequency EPR evidence for a bimetallic center at the Cu_A site in cytochrome *c* oxidase, FEBS Lett. 268 (1) (1990) 274–276.

[144] H.J. Hwang, Y. Lu, pH-dependent transition between delocalized and trapped valence states of a CuA center and its possible role in proton-coupled electron transfer, Proc. Natl. Acad. Sci. U. S. A. 101 (35) (2004) 12842.

[145] D. Lukoyanov, S.M. Berry, Y. Lu, W.E. Antholine, C.P. Scholes, Role of the coordinating histidine in altering the mixed valency of Cu_A: an electron nuclear double resonance-electron paramagnetic resonance investigation, Biophys. J. 82 (5) (2002) 2758–2766.

[146] X. Xie, et al., Perturbations to the geometric and electronic structure of the Cu_A site: factors that influence delocalization and their contributions to electron transfer, J. Am. Chem. Soc. 130 (15) (2008) 5194–5205.

[147] O. Farver, H.J. Hwang, Y. Lu, I. Pecht, Reorganization energy of the CuA center in purple azurin: impact of the mixed valence-to-trapped valence state transition, J. Phys. Chem. B 111 (24) (2007) 6690–6694.

[148] H.J. Hwang, S.M. Berry, M.J. Nilges, Y. Lu, Axial methionine has much less influence on reduction potentials in a Cu_A center than in a blue copper center, J. Am. Chem. Soc. 127 (20) (2005) 7274–7275.

[149] H. Li, S.P. Webb, J. Ivanic, J.H. Jensen, Determinants of the relative reduction potentials of type-1 copper sites in proteins, J. Am. Chem. Soc. 126 (25) (2004) 8010–8019.

[150] F. John, L.D. Kanbi, W. Richard, S.S. Hasnain, Role of the axial ligand in type 1 Cu centers studied by point mutations of Met148 in rusticyanin, Biochemistry 38 (39) (1999) 12675–12680.

[151] J.A. Farrar, et al., The electronic structure of Cu_A: a novel mixed-valence dinuclear copper electron-transfer center, J. Am. Chem. Soc. 118 (46) (1996) 11501–11514.

[152] S.I. Gorelsky, X. Xie, Y. Chen, A. James, E.I. Solomon, The two-state issue in the mixed-valence binuclear Cu_A center in cytochrome *c* oxidase and N_2O reductase, J. Am. Chem. Soc. 128 (51) (2006) 16452–16453.

[153] F. Neese, W.G. Zumft, W.E. Antholine, P.M.H. Kroneck, The purple mixed-valence CuA center in nitrous-oxide reductase: EPR of the copper-63-, copper-65-, and both copper-65-and [^{15} N] histidine-enriched enzyme and a molecular orbital interpretation, J. Am. Chem. Soc. 118 (36) (1996) 8692–8699.

[154] F. Neese, R. Kappl, J. Hüttermann, W.G. Zumft, P.M.H. Kroneck, Probing the ground state of the purple mixed valence Cu_A center in nitrous oxide reductase: a CW ENDOR (X-band) study of the ^{65}Cu, ^{15}N-histidine labeled enzyme and interpretation of hyperfine couplings by molecular orbital calculations, J. Biol. Inorg. Chem. 3 (1) (1998) 53–67.

[155] L.A. Abriata, G.N. Ledesma, R. Pierattelli, A.J. Vila, Electronic structure of the ground and excited states of the Cu_A site by NMR spectroscopy, J. Am. Chem. Soc. 131 (5) (2009) 1939–1946.

[156] M.H.M. Olsson, U. Ryde, Geometry, reduction potential, and reorganization energy of the binuclear Cu_A site, studied by density functional theory, J. Am. Chem. Soc. 123 (32) (2001) 7866–7876.

[157] D.R. Gamelin, et al., Spectroscopy of mixed-valence Cu_A-type centers: ligand-field control of ground-state properties related to electron transfer, J. Am. Chem. Soc. 120 (21) (1998) 5246–5263.

[158] S.D.B. George, et al., A quantitative description of the ground-state wave function of Cu_A by X-ray absorption spectroscopy: comparison to plastocyanin and relevance to electron transfer, J. Am. Chem. Soc. 123 (24) (2001) 5757–5767.

[159] M.T. Giudici-Orticoni, F. Guerlesquin, M. Bruschi, W. Nitschke, Interaction-induced redox switch in the electron transfer complex rusticyanin-cytochrome c_4, J. Biol. Chem. 274 (43) (1999) 30365–30369.

[160] I. Díaz-Moreno, A. Díaz-Quintana, S. Díaz-Moreno, G. Subías, M.A. De la Rosa, Transient binding of plastocyanin to its physiological redox partners modifies the copper site geometry, FEBS Lett. 580 (26) (2006) 6187–6194.

[161] L. Wang, D.H. Waldeck, Denaturation of cytochrome c and its peroxidase activity when immobilized on SAM films, J. Phys. Chem. C 112 (5) (2008) 1351–1356.

[162] V.E. Kagan, et al., Cytochrome *c*/cardiolipin relations in mitochondria: a kiss of death, Free Radic. Biol. Med. 46 (11) (2009) 1439–1453.